

# Preheated shock experiments in the molten $\text{CaAl}_2\text{Si}_2\text{O}_8$ - $\text{CaFeSi}_2\text{O}_6$ - $\text{CaMgSi}_2\text{O}_6$ ternary: A test for linear mixing of liquid volumes at high pressure and temperature

Claire W. Thomas<sup>1</sup> and Paul D. Asimow<sup>1</sup>

Received 1 April 2013; revised 21 June 2013; accepted 25 June 2013; published 24 July 2013.

[1] We performed 17 new shock wave experiments on preheated (1673 K) hedenbergite liquid ( $\text{CaFeSi}_2\text{O}_6$ ) and two model basalt liquids (an equimolar binary mix of  $\text{CaAl}_2\text{Si}_2\text{O}_8$  +  $\text{CaFeSi}_2\text{O}_6$  and an equimolar ternary mix of  $\text{CaAl}_2\text{Si}_2\text{O}_8$  +  $\text{CaFeSi}_2\text{O}_6$  +  $\text{CaMgSi}_2\text{O}_6$ ) in order to determine their equations of state (EOS). Ambient pressure density measurements on these and other Fe-bearing silicate liquids indicate that FeO has a partial molar volume that is highly dependent on composition, which leads to large errors in estimates of the densities of Fe-bearing liquids at ambient pressure based on an ideal mixing of any fixed set of end-member liquids. We formulated a series of mixing tests using the EOS determined in this study to examine whether ideal mixing of volumes might nevertheless suffice to describe the ternary system  $\text{CaAl}_2\text{Si}_2\text{O}_8$ - $\text{CaFeSi}_2\text{O}_6$ - $\text{CaMgSi}_2\text{O}_6$  at high temperature and pressure. The ideal mixing null hypothesis is rejected; compositional variations in partial molar volume of FeO appear to extend to high pressure. Only densities of Fe-bearing liquid mixtures with oxide mole fraction of FeO less than 0.06 can be adequately approximated using an ideal solution.

**Citation:** Thomas, C. W., and P. D. Asimow (2013), Preheated shock experiments in the molten  $\text{CaAl}_2\text{Si}_2\text{O}_8$ - $\text{CaFeSi}_2\text{O}_6$ - $\text{CaMgSi}_2\text{O}_6$  ternary: A test for linear mixing of liquid volumes at high pressure and temperature, *J. Geophys. Res. Solid Earth*, 118, 3354–3365, doi:10.1002/jgrb.50269.

## 1. Introduction

[2] Silicate liquids play a large role in our understanding of both the early and modern Earth. Most widely accepted scenarios for the evolution of the early Earth involve at least one stage of extensive or complete melting, for example in the aftermath of impacts with large proto-planetary-sized objects such as the presumed moon-forming event [Canup, 2004, 2012; Canup and Asphaug, 2001; Čuk and Stewart, 2012]. The chemical and thermal evolution of the early molten mantle and how it affects the chemistry and physical properties of the modern mantle are not well understood. Furthermore, seismic observations of the 410 km discontinuity in the upper mantle [Revenaugh and Sipkin, 1994; Song et al., 2004] and ultralow velocity zones in the lowermost mantle [Garnero and Helmberger, 1995; Williams and Garnero, 1996] have been interpreted to indicate the presence of a neutrally buoyant partial melt, yet there is currently limited knowledge of how the density and compressibility of complex silicate liquids behave at high temperature and pressure. It is therefore essential to have experimental constraints on the equation

of state (EOS) of the complex multicomponent silicate liquids that would be actually present in nature. The difficulty lies in that natural silicate liquids comprise a potentially infinite, multidimensional continuum of compositions. Understanding their range of volumetric behavior requires either data on an arbitrarily large number of experiments or data on a minimum set of end-member compositions along with a reliable tool of interpolating among them. Choosing the correct method of interpolation is key to producing a predictive model for silicate liquid density and compressibility over a wide range of pressure, temperature, and composition space. Experimental data that provide constraints on end-member volumes as well as a few intermediate compositions offer the opportunity to test whether available methods for such interpolation are reliable.

[3] Ideal mixing of volumes has proven to be a reliable method of interpolation for ambient pressure experiments within a given composition and temperature range [Bottinga and Weill, 1970; Bottinga et al., 1982; Bottinga et al., 1983; Guo et al., 2013; Lange, 1997; Lange and Carmichael, 1990; Mo et al., 1982; Nelson and Carmichael, 1979], although exceptions from ideality exist and are discussed below. Likewise, ideal mixing silicate liquid volumes at high pressure has been employed as a simplifying assumption, but it in fact remains poorly tested and constrained [Asimow and Ahrens, 2010]. In this study, we report 17 new shock wave experiments to pressures up to 146 GPa on preheated silicate liquids of three separate compositions: hedenbergite (Hd;  $\text{CaFeSi}_2\text{O}_6$ ), a 50–50 mixture of anorthite and hedenbergite (An-Hd;

<sup>1</sup>Geological and Planetary Sciences, California Institute of Technology, Pasadena, California, USA.

Corresponding author: C. W. Thomas, Geological and Planetary Sciences, California Institute of Technology, 1200 E. California Blvd, MC 170-25, Pasadena, CA 91106, USA. (cwallier@gps.caltech.edu)

©2013. American Geophysical Union. All Rights Reserved. 2169-9313/13/10.1002/jgrb.50269

**Table 1.** Shock Compression Data

Shot #	Flyer Material	T (K)	$u_{fp}$ km s <sup>-1</sup>	±	$u_p$ km s <sup>-1</sup>	±	$U_s$ km s <sup>-1</sup>	±	$\rho_H$ Mg m <sup>-3</sup>	±	$P_H$ GPa	±
<i>Hedenbergite</i>												
1068 <sup>a</sup>	Mo	1673	1.976	0.002	1.58	0.01	5.12	0.11	4.27	0.05	23.8	0.4
413	Al	1673	4.471	0.002	2.006	0.005	5.56	0.07	4.62	0.04	32.9	0.3
419	Mo	1674	3.497	0.001	2.68	0.02	6.59	0.24	4.99	0.17	52.2	1.5
418	Mo	1673	4.066	0.148	3.05	0.01	7.50	0.06	4.98	0.03	67.6	0.4
417	Ta	1677	4.535	0.005	3.65	0.01	8.29	0.10	5.29	0.05	89.1	0.6
416	Ta	1672	5.144	0.012	4.10	0.01	9.01	0.09	5.42	0.06	109.1	0.9
415	Ta	1673	5.613	0.001	4.46	0.01	9.46	0.05	5.59	0.03	124.5	0.5
414	Ta	1675	6.187	0.020	4.88	0.01	10.10	0.05	5.72	0.03	145.6	0.9
<i>An-Hd</i>												
1070 <sup>a</sup>	Mo	1673	2.006	0.003	1.62	0.01	5.17	0.12	4.04	0.05	23.2	0.4
1074 <sup>a</sup>	Mo	1673	1.456	0.002	1.211	0.014	4.27	0.28	3.87	0.13	14.3	0.8
466	Mo	1675	3.618	0.003	2.82	0.01	6.56	0.15	4.87	0.10	51.3	0.9
469	Mo	1673	4.700	0.003	3.55	0.01	7.99	0.10	4.99	0.06	78.7	0.8
471	Mo	1674	5.815	0.016	4.37	0.01	8.66	0.11	5.59	0.08	104.8	1.0
<i>An-Hd-Di</i>												
1069 <sup>a</sup>	Mo	1673	2.016	0.003	1.63	0.03	5.48	0.47	3.88	0.10	24.4	2.1
1071 <sup>a</sup>	Mo	1673	1.470	0.005	1.20	0.01	4.77	0.30	3.64	0.09	15.6	0.8
468	Mo	1673	3.503	0.008	2.70	0.01	7.00	0.07	4.43	0.03	51.5	0.4
470	Mo	1674	4.796	0.006	3.61	0.02	8.31	0.16	4.81	0.09	81.7	1.3

<sup>a</sup>Caltech 40 mm propellant.

CaAl<sub>2</sub>Si<sub>2</sub>O<sub>8</sub>-CaFeSi<sub>2</sub>O<sub>6</sub>), and an equal mixture of anorthite, hedenbergite, and diopside (An-Hd-Di; CaAl<sub>2</sub>Si<sub>2</sub>O<sub>8</sub>-CaFeSi<sub>2</sub>O<sub>6</sub>-CaMgSi<sub>2</sub>O<sub>6</sub>). Determination of the EOS of Hd and the two mixtures (or “model basalts”) permits us to test the validity of linear mixing of volumes and ideal configurational mixing of entropies — two assumptions which were both used in *Thomas et al.* [2012] and *Thomas* [2013] to predict the volumes of multicomponent liquids at high  $T$  and  $P$ .

## 2. Methods

### 2.1. Sample Preparation

[4] The synthesis and analysis for the Hd and model basalt samples used in this study are described in *Guo et al.* [2013] and *Guo* [2013], respectively. These studies also describe the 1-bar double-bob Archimedean density measurements and the ultrasonic sound speed measurements that were completed on these materials. The sample materials used for the shock wave experiments were cored directly from the lower buffer rod crucible used in the sound speed determinations. The cores were sliced into disks, which were then lapped down to under-fill the volume of the molybdenum shock-experiment sample holder. The Mo sample holders are assembled from two machined pieces: (1) the driver plate, which has a hollow cylindrical projection on one side that becomes the sample well and (2) the cap, which is a 1 mm thick, 8 mm diameter disk that is welded on after filling (for complete description of the welding process see *Thomas et al.* [2012]). The interior volume of the sample well is 8 mm in diameter and 2.5 mm deep. The samples under-filled this volume by 7–13% at room temperature to prevent the welded cap from bowing during heating [c.f. *Thomas et al.*, 2012]

[5] The surfaces within the sample well including the inside surface of the cap were polished to a mirror finish with 1 micron alumina grit. Smoothing all the surfaces prevents

bubbles from clinging to the walls of the sample holder during heating and potentially interfering with the imaged shock wave. The outer surface of the cap was left with the finish quality as-machined (~9 micron finish), in order to match the quality of polish on the inner portion of the rear face of the driver plate, which was polished on a rotating stage. The speed of the polishing pad decreases towards the center; hence, the quality of mirror finish also decreases. Approximately, similar finishes on the cap and driver reflecting surfaces ease acquisition of evenly illuminated images of the cap and driver during the shot and greatly increased the precision of the Hd data given below. On the contrary, the model basalt capsules were polished as in the manner as described in *Thomas et al.* [2012] due to the larger quantity of light needed for the digital recording system [c.f. *Thomas*, 2013] (see Chapter 3). Hence, this data set is plagued with larger errors derived from determining the driver and cap arrivals with different exposure levels. Additional sample preparations are detailed in *Asimow and Ahrens* [2010], and *Thomas et al.* [2012].

### 2.2. Experimental Setup

[6] The pioneering work for shock studies on molten materials is *Rigden et al.* [1984]. The description of our methods below builds on this and the work of *Rigden et al.* [1988, 1989], *Miller et al.* [1988, 1991], *Chen and Ahrens* [1998], and *Chen et al.* [2002]. The most recent changes to experimental techniques and data analysis are in *Asimow et al.* [2008], *Asimow and Ahrens* [2010], and *Thomas et al.* [2012].

[7] For this study, 17, total experiments were performed—12 in the Caltech 90/25 mm two-stage light gas gun and five using the Caltech 40-mm propellant gun—eight performed on Hd, five performed on An-Hd, and four performed on An-Hd-Di (see Table 1). All shots were preheated to 1673 K ± 4 K (1400°C) and used either molybdenum (Mo),

**Table 2.** Parameters Used

	Molybdenum <sup>a</sup> (2273 K)	Molybdenum <sup>a</sup> (300 K)	Tantalum <sup>b</sup> (300 K)	Aluminum 2024 <sup>c</sup> (300 K)
$\rho_o$ Mg m <sup>-3</sup>	9.785	10.21	16.65	2.78
$C_o$ km s <sup>-1</sup>	4.858	5.033	3.293	5.330
$s$	1.288	1.289	1.307	1.34

<sup>a</sup>Asimow et al. [2008], Chase [1998];

<sup>b</sup>Mitchell and Nellis [1981];

<sup>c</sup>Marsh [1980].

tantalum (Ta), or aluminum alloy (Al2024) flyer plates. Flyer plate velocities ( $u_{fp}$ ) ranged from 1.46 to 6.19 km/s; the methods used for measuring  $u_{fp}$  are given in Chapter 3 of Thomas [2013]

[8] During each experiment, the rear face of the target is illuminated by a Specialized Imaging xenon spark lamp and filmed by a Hadland Imacon 790 streak camera through a narrow (25  $\mu$ m) slit focused horizontally across the center of the driver and sample cap. Hd shots were recorded on Polaroid film; the model basalts were recorded using a digital system [c.f. Thomas, 2013]. As the shock wave reaches the free surface of the driver or the cap, the reflected light from the polished surface is extinguished (or shows a sharp change in intensity). The offset time of these two cutoffs allows for the precise measurement of the shock transit time through the sample and molybdenum cap.

[9] To correct for nonuniform streaking rate, the camera was calibrated using a test streak image modulated by a radio-frequency tuner at 148.9875 MHz for a 1500 ns streak length and by a pulse generator at 1.7870 MHz for a 5000 ns streak (shot 1068). Each pixel line on the shot streak record can then be converted to a time during the experiment, which permits the shock transit time through the sample to be calculated from the pixel distance between the two cutoffs on the film (or digital image). A detailed method for picking cutoffs and reducing the data is described in Thomas et al. [2012].

[10] The final calculated shock state — i.e., shock pressure ( $P_H$ ), shock density ( $\rho_H$ ), particle velocity ( $u_p$ ), and shock velocity ( $U_s$ ) — is solved for iteratively [Rigden et al., 1988] using measured shock wave travel time, impedance

matching, the Rankine-Hugoniot equations, Hugoniot data ( $\rho_o$ ,  $C_o$ , and  $s$ ) for the metal flyer plates and hot Mo driver (Table 2), and the initial density ( $\rho_o$ ) for each of the silicate liquids (see Tables 3, 4, and 5). An initial guess for the bulk sound speed ( $C_o$ ) and Hugoniot slope  $s$  is required to seed the iteration, but the converged result is independent of this assumption. Uncertainties in all derived parameters ( $U_s$ ,  $u_p$ ,  $P_H$ , and  $\rho_H$ ) were obtained from the uncertainties in the measured and standard parameters by analytical error propagation [c.f. I Jackson and Ahrens, 1979].

### 3. Results

[11] The shock wave data are reported in Table 1, including shot number, flyer material, the temperature prior to firing,  $u_{fp}$ ,  $u_p$ ,  $U_s$ ,  $\rho_H$ , and  $P_H$ .

[12] A Hugoniot is a series of peak shock states achieved by progressively stronger shocks in a material from the same initial condition [Ahrens, 1987]. The Hugoniot of a well-behaved material empirically forms a line in  $U_s$ - $u_p$  space, given to third order in strain by  $U_s = C_o + s u_p$  [Jeanloz, 1989]. The bulk sound speed of the material at room pressure,  $C_o$ , is given by the intercept; the slope ( $s$ ) is related to  $K'_S$ , the isentropic pressure derivative of the isentropic bulk modulus ( $K_{oS}$ ) by [Ruoff, 1967],

$$s = \frac{(K'_S + 1)}{4}. \quad (1)$$

#### 3.1. Hedenbergite (CaFeSi<sub>2</sub>O<sub>6</sub>) Liquid

[13] Figure 1 shows linear fits to the Hd shock data in  $U_s$ - $u_p$  space. An unweighted linear fit to all eight preheated hedenbergite liquid data points yields  $U_s = 2.587 \pm 0.142 + 1.55 \pm 0.04 u_p$  km/s ( $r^2 = 0.996$ ). The experimentally determined ultrasonic value of the bulk sound speed, 2.613  $\pm 0.016$  km/s [Guo et al., 2013], lies within the stated uncertainty of the bulk sound speed derived from the intercept of this fit, 2.587  $\pm 0.142$  km/s. This relationship indicates relaxed (liquid-like) — as opposed to un-relaxed (glass-like) — behavior upon shock compression [Rigden et al., 1988]. Therefore, to reduce the error on the linear fit, we fixed the intercept at the mean ultrasonic value yielding an unweighted

**Table 3.** Equation of State Fits for Molten CaFeSi<sub>2</sub>O<sub>6</sub><sup>a</sup>

	Units	SWEOS	BM3	BM4	Source
$T_o$	K	1673	1673	1673	
$\rho_o$	kg m <sup>-3</sup>	2913 $\pm$ 11	2913 $\pm$ 11	2913 $\pm$ 11	G13a
$C_o$	m s <sup>-1</sup>	2613 $\pm$ 16	-	-	G13a
$S$		1.54 $\pm$ 0.01	-	-	fitted
$\gamma_o$		0.300	0.300	0.300	derived
$Q$		-	-1.93 $\pm$ 0.41	0.47 $\pm$ 9.86	fitted
$K_{So}$	GPa	19.89 $\pm$ 0.24	19.89 $\pm$ 0.24	19.89 $\pm$ 0.24	derived
$K'_S$		5.16 $\pm$ 0.04	6.22 $\pm$ 0.55*	3.15 $\pm$ 1.61*	derived/*fitted
$K''_S$	GPa <sup>-1</sup>	-	-	0.78 $\pm$ 0.60	fitted
$\chi^2$		-	4.20	3.26	
$K_T$	GPa	19.32	19.32	19.32	derived
$A$	K <sup>-1</sup>	5.91-05	5.91-05	5.91-05	G13a
$C_p$	J kg <sup>-1</sup> K <sup>-1</sup>	1345.48	1345.48	1345.48	LN92
$C_v$	J kg <sup>-1</sup> K <sup>-1</sup>	11,306.70	11,306.70	11,306.70	derived

<sup>a</sup>SWEOS= shock wave equation of state. 3BM/MG = third-order Birch-Murnaghan/Mie-Grüneisen EOS 4BM/MG = fourth-order Birch-Murnaghan/Mie-Grüneisen EOS Sources: Fitted indicates an adjustable parameter, L97 is Lange [1997], LN92 is Lange and Navrotsky [1992], G13a is Guo et al. [2013].

**Table 4.** Equation of State Fits for Molten An-Hd<sup>a</sup>

	Units	SWEOS	BM3	BM4	Source
$T_o$	K	1673	1673	1673	
$\rho_o$	kg m <sup>-3</sup>	2772 $\pm$ 3	2772 $\pm$ 3	2772 $\pm$ 3	G13b
$C_o$	m s <sup>-1</sup>	2772 $\pm$ 11	-	-	G13b
$S$		1.39 $\pm$ 0.03	-	-	fitted
$\gamma_o$		0.310	0.310	0.310	derived
$Q$		-	-0.18 $\pm$ 2.25	1.67 $\pm$ 2.79	fitted
$K_{So}$	GPa	21.30 $\pm$ 0.25	21.30 $\pm$ 0.25	21.30 $\pm$ 0.25	derived
$K'_S$		4.54 $\pm$ 0.12	5.49 $\pm$ 0.65*	5.10 $\pm$ 1.61*	derived/*fitted
$K''_S$	GPa <sup>-1</sup>	-	-	-0.17 $\pm$ 0.82	fitted
$\chi^2$		-	6.37	12.53	
$K_T$	GPa	20.68	20.68	20.68	derived
$A$	K <sup>-1</sup>	5.81-05	5.81-05	5.81-05	G13b
$C_p$	J kg <sup>-1</sup> K <sup>-1</sup>	1442.34	1442.34	1442.34	LN92
$C_v$	J kg <sup>-1</sup> K <sup>-1</sup>	11,400.19	11,400.19	11,400.19	derived

<sup>a</sup>Sources: Fitted indicates an adjustable parameter, L97 is Lange [1997], LN92 is Lange and Navrotsky [1992], G13b is Guo et al. [2013].

**Table 5.** Equation of State Fits for Molten An-Hd-Di<sup>a</sup>

	Units	SWEOS	BM3	Source
$T_o$	K	1673	1673	
$\rho_o$	kg m <sup>-3</sup>	2722 ± 2	2722 ± 2	G13b
$C_o$	m s <sup>-1</sup>	2846 ± 14	-	G13b
$S$		1.54 ± 0.02	-	fitted
$\gamma_o$		0.361	0.361	derived
$Q$		-	-1.14 ± 0.79	fitted
$K_{So}$	GPa	22.03 ± 0.25	22.03 ± 0.25	derived
$K'_S$		5.15 ± 0.06	6.20 ± 0.17*	derived/*fitted
$K''_S$	Gpa <sup>-1</sup>	-	-	fitted
$\chi^2$		-	0.39	
$K_T$	Gpa	21.19	21.19	derived
$A$	K <sup>-1</sup>	6.64-05	6.64-05	G13b
$C_p$	J kg <sup>-1</sup> K <sup>-1</sup>	1491.96	1491.96	LN92
$C_v$	J kg <sup>-1</sup> K <sup>-1</sup>	11,434.47	11,434.47	derived

<sup>a</sup>For abbreviations, see Tables 3 and 4.

constrained linear fit of  $U_S = 2.613 \pm 0.016 + 1.54 \pm 0.01 u_p$  km/s ( $r^2 = 0.999$ ).

[14] It is necessary to select and apply a thermal equation of state formalism for investigating material properties that lie off the Hugoniot, since the Hugoniot achieves temperatures and energies much higher than those of geophysical interest at lower mantle pressures (even for processes during early Earth differentiation). We have defined the entire  $P$ - $V$ - $E$  surface of hedenbergite liquid using various formalisms: the shock wave equation of state (SWEOS) and the third- and fourth-order Birch-Murnaghan Mie-Grüneisen EOS (3BM/MG and 4BM/MG). For a full description of the thermal EOS equations and fitting procedures, the reader is directed to *Asimow and Ahrens [2010]* and *Thomas et al. [2012]*. The results and uncertainties for each fit on Hd are given in Table 3, and the Hugoniot are plotted in Figure 2.

[15] The SWEOS is defined by a linear Hugoniot in  $U_S$ - $u_p$  space, converted to  $P$  -  $\rho$  space using the first and second Rankine-Hugoniot equations [e.g., *Ahrens, 1987*]. States that lie off the Hugoniot are found using the Mie-Grüneisen thermal pressure approximation with

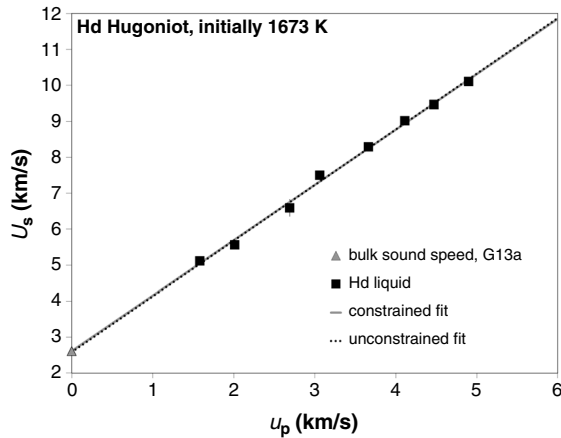


**Figure 1.** Preheated (1673 K) CaFeSi<sub>2</sub>O<sub>6</sub> liquid Hugoniot in shock velocity ( $U_S$ )-particle velocity ( $u_p$ ) space. The dotted line represents the unconstrained linear Hugoniot; G13a is *Guo et al. [2013]*.

a temperature-independent power law expression for the thermodynamic Grüneisen parameter

$$\gamma(\rho) = \gamma_o \left( \frac{\rho_o}{\rho} \right)^q. \quad (2)$$

[16] Although a value for  $q$  to be used with the SWEOS was not independently determined in this study, experimental results thus far indicate that silicate liquids—including iron-bearing liquids [*Thomas et al., 2012*—appear to have  $q$  values of  $-0.88$  to  $-2$  for compressions of  $1 > \rho_o/\rho > 0.49$ . The slope and intercept of the constrained Hugoniot fit given above correspond to a  $K'_S$  value of  $5.16 \pm 0.04$  derived from (1) and a  $K_{oS}$  value of  $19.98 \pm 0.24$  GPa derived from the expression

$$C_o = \sqrt{\frac{K_{oS}}{\rho_o}}. \quad (3)$$

[17] The third- or fourth-order BM/MG EOS is defined by a third- or fourth-order Birch-Murnaghan isentrope centered at 1 bar and 1673 K and a Mie-Grüneisen thermal pressure approximation. The 3BM/MG fit result is  $K'_S = 6.22 \pm 0.55$ ,  $q = -1.93 \pm 0.41$ , and reduced  $\chi^2 = 4.20$ . The 4BM/MG fit result is  $K'_S = 3.15 \pm 1.67$ ,  $K''_S = 0.78 \pm 0.60$  GPa<sup>-1</sup>,  $q = 0.47 \pm 9.86$  and reduced  $\chi^2 = 3.26$ . The high precision for most of the points in the Hd data set propagates into unusually high  $\chi^2$  values for both fits. Nevertheless, comparatively, the 4BM/MG has very large error bars on and strong correlations among the output parameters indicating a very unstable fitting routine. The 3BM/MG fit, by contrast, has less severe correlation between the parameters and appears justified by the fitting statistics. Hence for this data set, we prefer the third-order fit.

### 3.2. An-Hd Liquid

[18] The An-Hd Hugoniot in  $U_S$ - $u_p$  space is shown in Figure 3. The unweighted linear fit is  $U_S = 2.742 \pm 0.282 + 1.40 \pm 0.09 u_p$  km/s ( $r^2 = 0.986$ ). As observed above for Hd liquid, the An-Hd liquid appears to be relaxed upon compression as the experimentally determined bulk sound speed,  $2.772 \pm 0.011$  km/s [*Guo et al., 2013*], and the intercept are within error. We can then fix the intercept at the mean

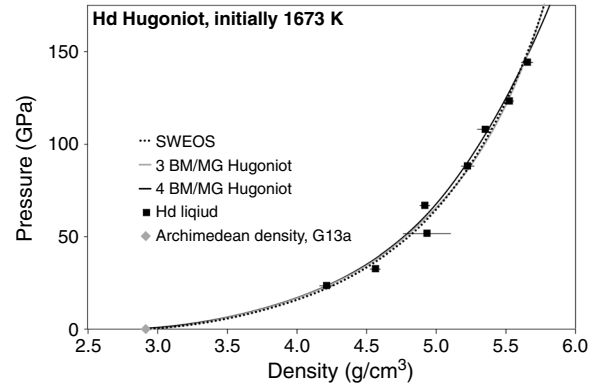


**Figure 2.** CaFeSi<sub>2</sub>O<sub>6</sub> liquid Hugoniot plotted in pressure-density space with thermal EOS fits. Data symbols are the same as Figure 1. Abbreviations: SWEOS—shock wave equation of state; BM/MG—Birch-Murnaghan/Mie-Grüneisen EOS. G13a is *Guo et al. [2013]*.

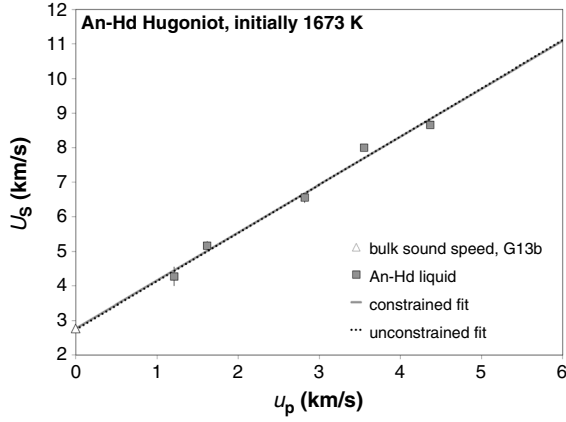


**Figure 3.** Preheated (1673 K) An-Hd liquid Hugoniot in shock velocity ( $U_S$ )-particle velocity ( $u_p$ ) space. The dotted line represents the unconstrained linear Hugoniot. G13b is *Guo et al.* [2013].

ultrasonic value yielding an unweighted constrained linear fit of  $U_S = 2.772 \pm 0.011 + 1.39 \pm 0.03 u_p$  km/s ( $r^2 = 0.998$ ). This slope and intercept constrain the SWEOS  $K'_S$  and  $K_{oS}$  values to be  $4.54 \pm 0.12$  and  $21.30 \pm 0.25$  GPa, respectively.

[19] The 3BM/MG fit result is  $K'_S = 5.49 \pm 0.65$ ,  $q = -0.18 \pm 2.25$ , and reduced  $\chi^2 = 6.37$ . The 4BM/MG fit result is  $K'_S = 5.10 \pm 1.61$ ,  $K''_S = -0.17 \pm 0.60$  GPa $^{-1}$ ,  $q = 1.67 \pm 2.79$  and reduced  $\chi^2 = 12.53$ . Both fits have relatively large error bars and large reduced  $\chi^2$  due to the low number of data points and fairly significant scatter in  $P$ - $\rho$  space (Figure 4). Yet both fits give similar  $K'_S$  to SWEOS, which is well defined by the linear fit. We therefore prefer the third-order fit despite having large errors, since it fits the data sufficiently well, has a lower reduced  $\chi^2$  and exhibits a negative  $q$  value, which has been shown to be typical for silicate liquids [Thomas, 2013]. The EOS parameters and their uncertainties for An-Hd liquid are given in Table 4.

### 3.3. An-Hd-Di Liquid

[20] The An-Hd-Di Hugoniot in  $U_S$ - $u_p$  space is shown in Figure 5. The unweighted linear fit is  $U_S = 2.823 \pm 0.197 + 1.52 \pm 0.09 u_p$  km/s ( $r^2 = 0.995$ ). Behaving as the two liquids above, An-Hd-Di liquid is relaxed upon compression [Guo,

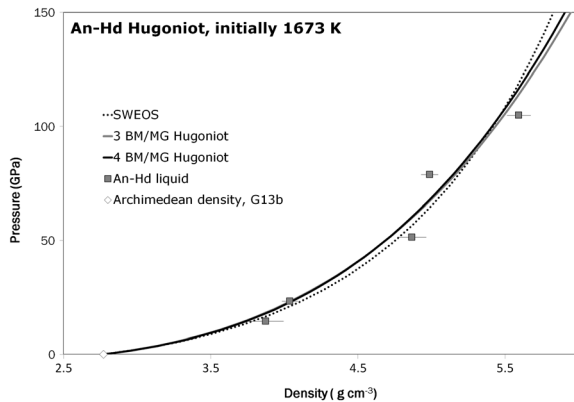


**Figure 4.** An-Hd liquid Hugoniot plotted in pressure-density space with thermal EOS fits. The abbreviations are the same as Figures 2 and 3.

2013], which justifies an unweighted constrained linear fit of  $U_S = 2.846 \pm 0.014 + 1.54 \pm 0.02 u_p$  km/s ( $r^2 = 0.999$ ). This slope and intercept constrain the SWEOS  $K'_S$  and  $K_{oS}$  values to be  $5.15 \pm 0.06$  and  $22.03 \pm 0.25$  GPa, respectively.

[21] The An-Hd-Di liquid was fit only with the 3BM/MG, as fitting the 4BM/MG to so few data points is under-constrained and does not yield a meaningful reduced  $\chi^2$ . The 3BM/MG result is  $K'_S = 6.20 \pm 0.17$ ,  $q = -1.14 \pm 0.79$ , and reduced  $\chi^2 = 0.39$ . The results and uncertainties for each fit on An-Hd-Di are given in Table 5, and the Hugoniots are plotted in Figure 6.

## 4. Discussion

### 4.1. Linear Mixing Assumptions

[22] To make progress on calculating the volumetric properties of the natural multicomponent silicate liquids that may occur in the lower mantle, the plan has been to constrain the EOS for a number of important end-member liquids using shock wave studies and then to attempt to reliably interpolate among them. End-member liquids that have been determined previously using shock wave methods are:  $\text{Fe}_2\text{SiO}_4$  (Fa, fayalite),  $\text{Mg}_2\text{SiO}_4$  (Fo, forsterite),  $\text{MgSiO}_3$  (En, enstatite),  $\text{CaAl}_2\text{Si}_2\text{O}_8$  (An, anorthite), and  $\text{CaMgSi}_2\text{O}_6$  (Di, diopside). The recommended EOS parameters for each of these end-members are given in Chapter 3 of Thomas [2013]. In Thomas *et al.* [2012], these five end-members were used to interpolate within the CaO-MgO-Al $_2$ O $_3$ -SiO $_2$ -FeO major element component space to constrain the volume of a liquid along an isentropic temperature-pressure path for a desired composition, yet there was not a clear test of the validity of the two underlying assumptions: (1) linear mixing of volumes and (2) constant entropy of mixing for a given composition.

[23] The assumption of linear or ideal mixing is simplest assumption that can be made for mixtures,

$$V_{\text{tot}} = \sum_i X^i V^i + V_{\text{mix}}, \quad (4)$$

where the volume of mixing ( $V_{\text{mix}}$ ) is assumed to be zero, and hence the total volume ( $V_{\text{tot}}$ ) is just a linear combination of the end-member partial molar volumes ( $V^i$ ) multiplied by

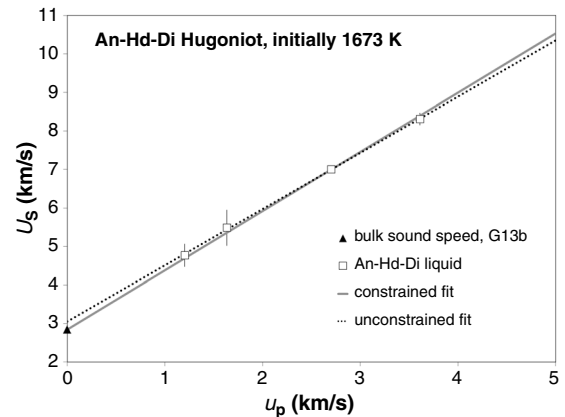


**Figure 5.** Preheated (1673 K) An-Hd-Di liquid Hugoniot in shock velocity ( $U_S$ )-particle velocity ( $u_p$ ) space. The dotted line represents the unconstrained linear Hugoniot. G13b is *Guo et al.* [2013].

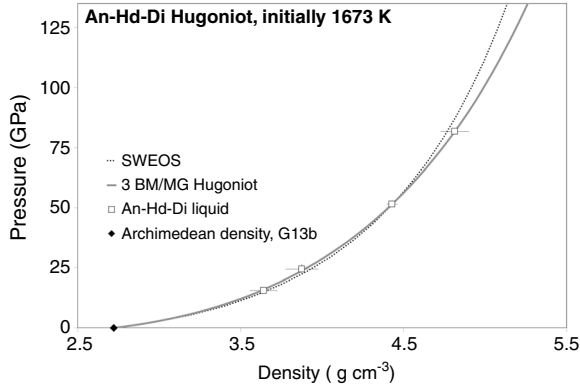


**Figure 6.** An-Hd-Di liquid Hugoniot plotted in pressure-density space with thermal EOS fits. The abbreviations are the same as Figures 2 and 5.

their respective mole fractions ( $X^i$ ). The second assumption is that the configurational entropy of a liquid solution is a function of composition only and therefore does not change with variations in temperature and pressure for a chosen liquid composition, such that

$$S_{tot} = \sum_i X^i S^i + S_{mix}, \quad (5)$$

where the entropy of mixing ( $S_{mix}$ ) is assumed to be a constant value for each composition and hence an isentrope or constant entropy path in  $T$ - $P$  space can be found from

$$dS_{tot} = d \sum_i X^i S^i = \sum_i X^i \left( C_p^i d \ln(T) - \frac{\partial V^i}{\partial T_P} dP \right) = 0, \quad (6)$$

where the  $T$  and  $P$  derivatives of entropy come from standard thermodynamic identities. Our data do not provide a test of this method of computing isentropes, since we lack experimentally defined isentropes for reference. Assuming configurational entropy to be function of composition only cannot be explicitly true if cation speciation is changing; hence, this serves only as our best approximation. We therefore focus on evaluating the volume of mixing assumption by comparing isentropes for intermediate compositions constructed with different sets of end-members, while acknowledging that this exercise may be compromised to some extent by the configurational entropy issue.

#### 4.2. Glass and 1 Bar Melt Data

[24] Both of these assumptions given in the section above have historically performed fairly well at 1 bar. Linear mixing of temperature-independent partial molar heat capacities has been a successful model for most silicate liquids [Stebbins *et al.*, 1984]. Similarly, linear mixing of volumes has been successful in determining silicate liquid densities in most major element space ( $\text{SiO}_2$ - $\text{Al}_2\text{O}_3$ - $\text{MgO}$ - $\text{CaO}$ - $\text{Na}_2\text{O}$ - $\text{K}_2\text{O}$ ) [Lange, 1997; Lange and Carmichael, 1990]. However, exceptions to both rules do exist. Heat capacities for the  $\text{Fe}_2\text{O}_3$  oxide component were shown to vary strongly with composition [Lange and Navrotsky, 1992], and the partial molar volumes of  $\text{Fe}_2\text{O}_3$  and  $\text{TiO}_2$  components are both variable with composition. These exceptions are attributed to the  $\text{Fe}^{3+}$  and  $\text{Ti}^{4+}$  cations having multiple coordination states at ambient pressure that are highly dependent on the

composition, i.e., fraction of non- $\text{SiO}_2$  components [Liu and Lange, 2001, 2006].

[25] More recent results have found this to be potentially true for  $\text{Fe}^{2+}$  as well, in that the partial molar volume of  $\text{FeO}$  ( $V_{\text{FeO}}$ ) in a melt is observed to depend on composition in some cases [Guo *et al.*, 2013]. Such behavior of  $\text{Fe}^{2+}$  is well documented in the glass literature, which is important insofar as glasses provide a proxy for structural properties of melt at the glass transition temperature. When discussing melt structure, language is typically borrowed from random network theory [Zachariasen, 1932], which distinguishes oxides as network formers, network modifiers, or intermediates. Network-forming cations (e.g.,  $\text{Si}^{4+}$ ) occur typically in tetrahedral ([4]) oxygen coordination in various connected units in the melt, whereas network modifiers (e.g.,  $\text{CaO}$ ,  $\text{MgO}$ ) typically occupy octahedrally ([6]) coordinated sites and disrupt the tetrahedral network. Intermediates (e.g.,  $\text{Al}_2\text{O}_3$ ,  $\text{TiO}_2$ ) can take on either role, may occupy multiple coordination sites, and may either disrupt or stabilize the polymerization of a melt [Bottinga and Weill, 1972; Mysen, 1983, 1988]. This is a simplified view of glasses and melts, but it acts to guide our intuition concerning the behavior of cations and the contributions of  $\text{Fe}^{3+}$  and  $\text{Ti}^{4+}$  to the density, heat capacity, and other thermodynamic properties of silicate melts [Burns, 1993; Mysen, 1988].

[26]  $\text{FeO}$  is an intermediate glass former and has been documented to take on a range of [4] to [6] coordination dependent on composition.  $\text{Fe}^{2+}$  is predominantly a network modifier in basaltic glasses [Burns, 1993; W E Jackson *et al.*, 2005; Mysen, 1983, 1988] and also likely in melts with

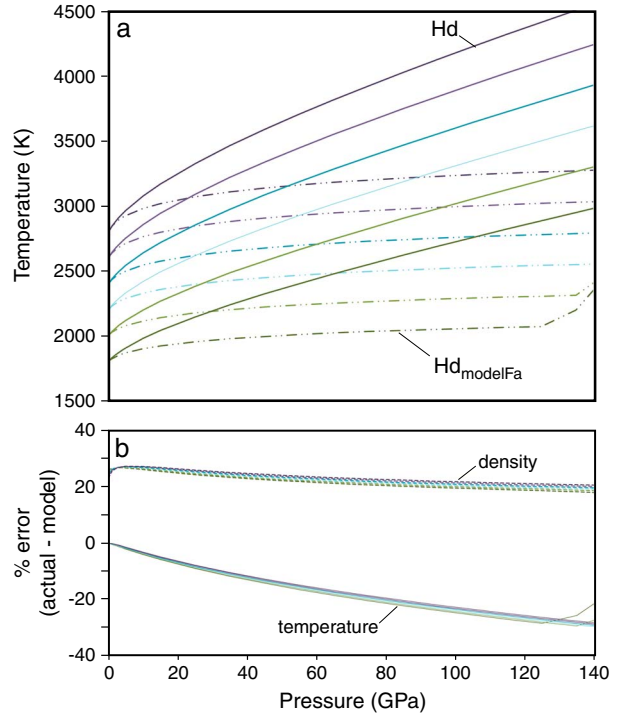


**Figure 7.** a) A comparison of the mixing model ( $\text{Hd}_{\text{modelFa}} = \text{Di} + 0.5 \text{Fa} - 0.5 \text{Fo}$ ) and the Hd isentrope at various potential temperatures ( $T_p$ ) and b) its % errors in temperature and density in estimating the Hd isentrope.

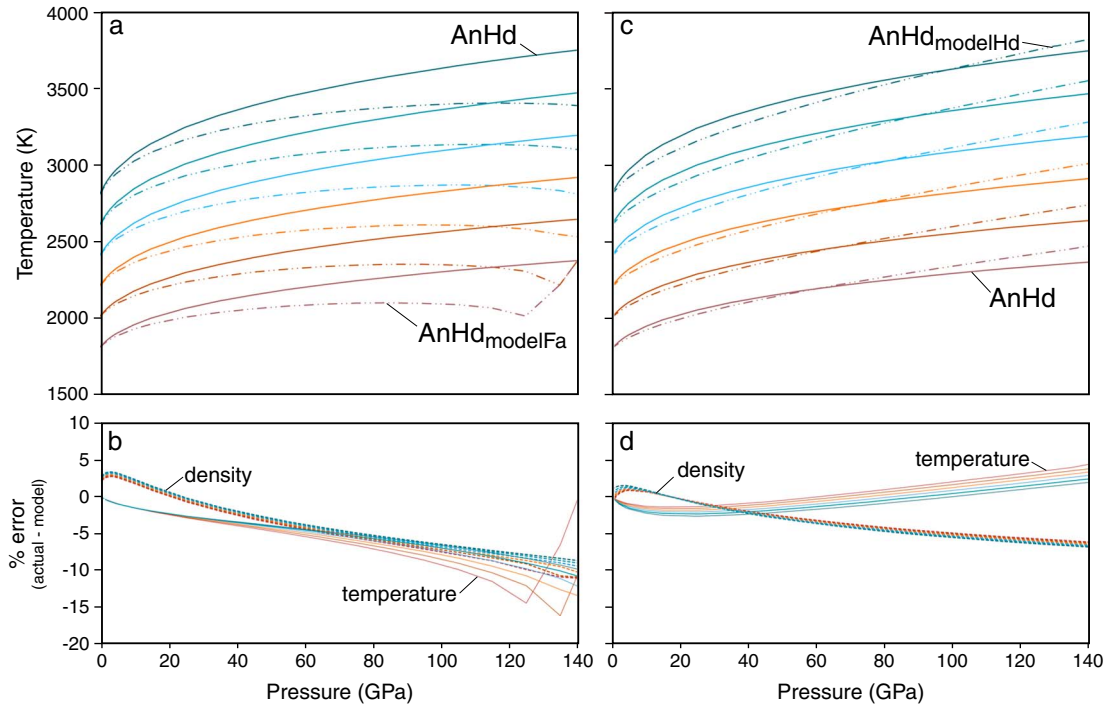


**Figure 8.** a) A comparison of the mixing model using a Fa end-member ( $\text{AnHd}_{\text{modelFa}} = 0.5 \text{ An} + 0.25 \text{ Fa} - 0.25 \text{ Fo} + 0.5 \text{ Di}$ ) and the An-Hd isentrope at various potential temperatures ( $T_p$ ) and b) its % errors in temperature and density in estimating the An-Hd isentrope. c) A comparison of the mixing model using an Hd end-member ( $\text{AnHd}_{\text{modelHd}} = 0.5 \text{ An} + 0.5 \text{ Hd}$ ) and the An-Hd isentrope at various potential temperatures ( $T_p$ ) and d) its % errors in temperature and density in estimating the An-Hd isentrope. Errors shown in text are the maximum at 120 GPa.

similar  $\text{SiO}_2$  mole fraction. This is supported by the relatively low 1 bar  $V_{\text{FeO}}$  value ( $\sim 12.1 \text{ cm}^3/\text{mol}$ ) for An-Hd, An-Di-Hd, and Hd-Di model basalts at 1732 K. This  $V_{\text{FeO}}$  has been inferred to indicate an average  $\text{Fe}^{2+}$  coordination of  $\sim [5.7]$  due to its similarity to the molar volume of wüstite, crystalline FeO (in which  $\text{Fe}^{2+}$  is octahedrally coordinated) [Guo *et al.*, 2013]. On the contrary,  $\text{Fe}_2\text{SiO}_4$  glasses contain very low-coordinated  $\text{Fe}^{2+}$  and are surprisingly polymerized [Cooney and Sharma, 1990]. X-ray absorption spectroscopy studies of both glass and melt of fayalite composition infer an average coordination of  $\sim [4]$  [W E Jackson *et al.*, 1993]. This is again supported by melt densities, where  $V_{\text{FeO}}$  increases to  $\sim 14\text{--}17 \text{ cm}^3/\text{mol}$  [Mo *et al.*, 1982; Shiraishi *et al.*, 1978; Thomas *et al.*, 2012], similar to the molar volume of crystalline  $\text{CaFeO}_2$ , a structure in which  $\text{Fe}^{2+}$  is [4] coordinated [Guo *et al.*, 2013].

[27] Between these two extremes, Hd and the CaO-FeO- $\text{SiO}_2$  (CFS) melts measured in Guo *et al.* [2013] display FeO in an average coordination state intermediate between [4] and [6]. The  $V_{\text{FeO}}$  for Hd melt ( $\sim 15.47 \text{ cm}^3/\text{mol}$ ) is inferred to indicate [4.7] coordination, similar to the values in Hd glasses ( $\sim 4.3$ ) and in molecular dynamics simulation of this melt [Rossano *et al.*, 2000]. The inferred coordination for CFS glasses range from 4.6 to 5.2. Guo *et al.* [2013] present an inverse correlation between CaO concentration and average  $\text{Fe}^{2+}$  coordination number. This is contrary to expectation from the model in Jackson *et al.* [2005] based on valence bond (VB) theory, which suggests a direct correlation between the concentration of network modifying

cations (those with higher bond valence with oxygen than Fe, i.e., Ca, Mg, Na, and Rb) and FeO coordination. For example in the VB model, Ca would have a greater “share” of the O valence due to the higher bond valence of the Ca-O bond and force Fe to find charge balance with other oxygens and hence increase coordination at a fixed Si content.

[28] Hence, the composition dependence of Fe coordination in CFS melts appears to be also strongly related to the degree of polymerization (Si/O ratio) [Burns, 1993] due to the intermediate nature of Fe. For example in Hd, where  $\text{SiO}_2$  is high (Si/O = 0.33) and there are equal proportions of CaO and FeO, FeO fills both roles of network former and modifier with an average value of [4.7]. For the family of CFS melts studies by Guo *et al.* [2013], the Fe content is fixed (40 mol %) and so increasing CaO is coupled to decreasing  $\text{SiO}_2$ ; therefore, the  $\text{Fe}^{2+}$  may be energetically forced to play the role of network former as CaO competes more effectively for octahedral sites. This competition would effectively lower the average Fe coordination, opposite of the effect predicted by the VB model. Qualitatively, one can understand the importance of FeO as an intermediate behavior cation when  $\text{Fe}_2\text{SiO}_4$  is compared to  $\text{Mg}_2\text{SiO}_4$  melt, which has the same low Si/O ratio (0.25). Since MgO acts only as network modifier and cannot act as a network former, Mg-rich melts typically have fully depolymerized structure and display very low viscosities [Urbain *et al.*, 1982]. For fayalite liquid, FeO is energetically favored as a network former to accommodate the charge balance of the oxygen, creating a highly polymerized glass as observed by Cooney and Sharma [1990].



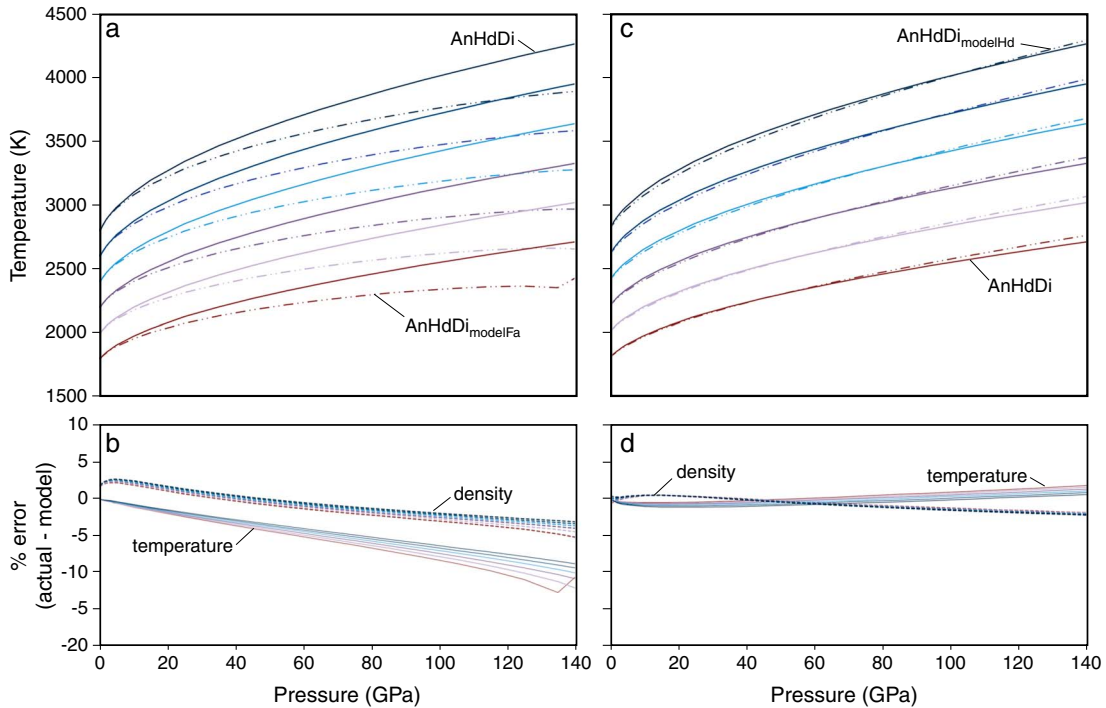


**Figure 9.** a) A comparison of the mixing model using a Fa end-member ( $\text{AnHdDi}_{\text{modelFa}} = 0.33 \text{ An} + 0.667 \text{ Di} + 0.167 \text{ Fa} - 0.167 \text{ Fo}$ ) and the An-Hd-Di isotrope at various potential temperatures ( $T_P$ ) and b) its % errors in temperature and density in estimating the An-Hd-Di isotrope. c) A comparison of the mixing model using an Hd end-member ( $\text{AnHdDi}_{\text{modelHd}} = 0.33 \text{ An} + 0.33 \text{ Hd} + 0.33 \text{ Di}$ ) and the An-Hd-Di isotrope at various potential temperatures ( $T_P$ ) and d) its % errors in temperature and density in estimating the An-Hd-Di isotrope. Errors shown in text are the maximum at 120 GPa.

[29] The dependence of FeO coordination and molar volume on other cation concentration invalidates the assumption of linear mixing of volumes at 1 bar for FeO-bearing liquids. It is unclear, however, what effect pressure and temperature may have. For glasses, higher temperatures are believed to decrease the coordination of transition metals [W E Jackson *et al.*, 2005], and there is some evidence that cations in melts will favor a coordination state lower than that of the glass [W E Jackson *et al.*, 1993]. At low pressure, network forming  $\text{SiO}_4$  tetrahedra predominate, but as  $P$  increases,  $\text{Si}^{4+}$  coordination increases ( $\sim 6.5$  at 150 GPa) [Karki *et al.*, 2007]. Less is known about the coordination of network modifiers at high pressure. Preliminary modeling of  $\text{Fe}_2\text{SiO}_4$  liquid shows decreasing Fe-O bond length and increasing coordination of Fe with pressure, but this does not constrain the effect of other cations [D. Muñoz Ramo and L. Stixrude, Spin crossover in  $\text{Fe}_2\text{SiO}_4$  liquid at high pressure, submitted to *Physical Review Letters*, 2013]. Guo *et al.* [2013] provides indirect evidence that coordination of  $\text{Fe}^{2+}$  in basaltic melts may decrease towards [5] at moderate pressures ( $\sim 5$  GPa).

[30] The only previous test of linear mixing at high pressure and temperature was for Fe-free anorthite-diopside liquids [Asimow and Ahrens, 2010], which found the linear approximation suitable at elevated  $T$ - $P$  conditions along the measured Hugoniot. Linear mixing appeared to fail at low temperatures, but this may have been an artifact of uncertainties in the large extrapolation downwards from the Hugoniot temperature. Another partial success for linear mixing was found in MD simulations of An-Di and also in MD simulations of the MgO-SiO<sub>2</sub> binary, each of which

showed well-behaved mixing at high pressure which began to break down at lower pressure [de Koker *et al.*, 2013; Martin *et al.*, 2012].

### 4.3. Tests of Linear Mixing

[31] Our first test examines whether the  $V_{\text{FeO}}$  difference between  $\text{Fe}_2\text{SiO}_4$  and  $\text{CaFeSi}_2\text{O}_6$  at 1 bar is still significant at high temperature and pressure. That is, can  $V_{\text{FeO}}$  for either end-member substitute for the other, as it would in the case of ideal mixing of volumes? To test this, we compare the Hd isotrope from shock wave experiments determined in this study to a modeled linear combination of end-member liquids, where  $\text{Hd}_{\text{modelFa}} = \text{Di} + 0.5 \text{ Fa} - 0.5 \text{ Fo}$ . The equations and details of creating isotropes of mixtures are given in Thomas *et al.* [2012]. The results are shown in Figure 7, where it is apparent that the model does not capture the behavior of the Hd isotrope. The errors for temperature and density are highly correlated such that if the model predicts a lower temperature than the actual isotrope, it will over predict the density and vice versa. Such is the case for Hd, where the errors at high pressure ( $\sim 120$  GPa) and temperature are maximized, and the model underestimates the temperature by 30% and overestimates the density by 20% (Figure 7b). A successful model for linear mixing would have errors for density of 1–2%, which is the average experimental error for a shock wave experiment. In this test, comparing the use of two Fe-rich end-members, we find a failure of linear mixing, and this is presumably due to complexity in the coordination state of  $\text{Fe}^{2+}$ .



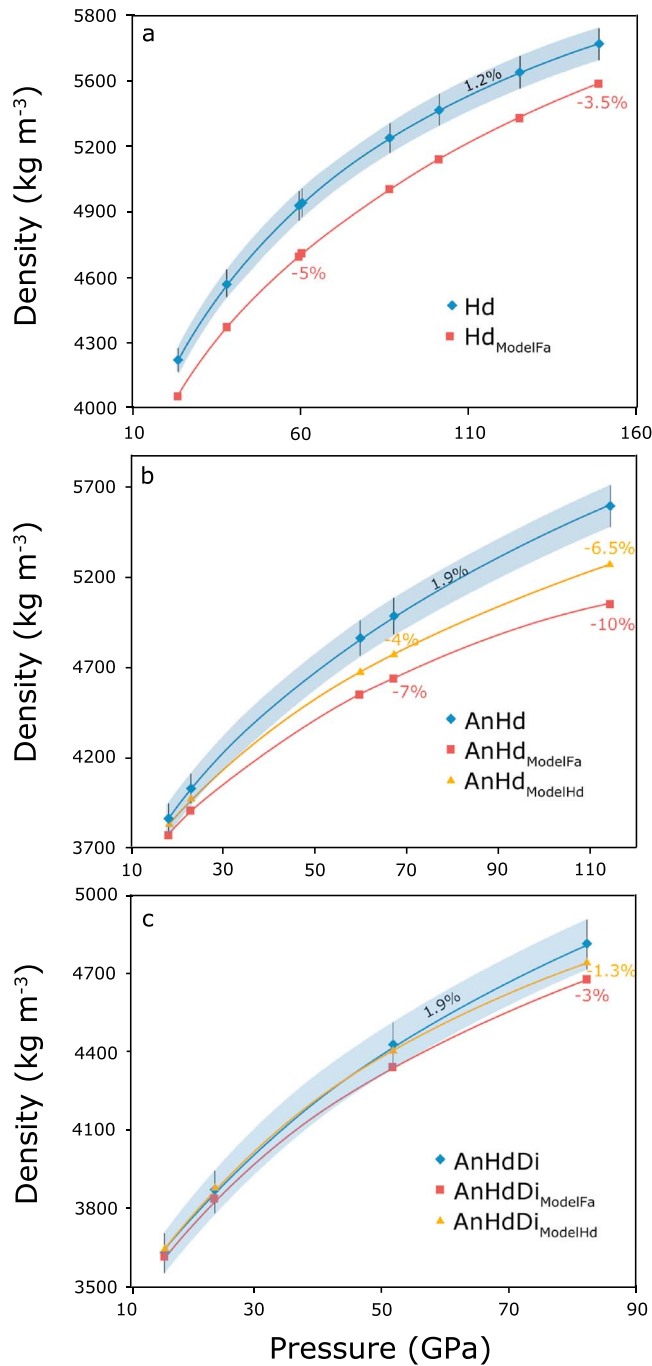


**Figure 10.** a) Mixing model along the Hd liquid Hugoniot, b) An-Hd liquid Hugoniot, and c) the An-Hd-Di liquid Hugoniot. Models used are given in Figures 7, 8, and 9. Each diamond corresponds to the EOS fit of an experimental point, and the error bars represent the average experimental error for that data set (1.2%, 1.9%, and 1.9% for Hd, An-Hd, and An-Hd-Di, respectively). The curves interpolate between the points, and the colored percentages represent the underestimation of each model to EOS fit.

[32] Our second test examines the question: Which model will perform better in creating an Fe-rich model basalt, An-Hd — using  $V_{\text{FeO}}$  derived from Fa or  $V_{\text{FeO}}$  derived from Hd? Our expectation from 1 bar coordination numbers is that Hd should be a better end-member for modeling An-Hd. Two mixing models,  $\text{AnHd}_{\text{modelFa}} = 0.5 \text{ An} + 0.25 \text{ Fa} - 0.25 \text{ Fo} + 0.5 \text{ Di}$  and  $\text{AnHd}_{\text{modelHd}} = 0.5 \text{ An} + 0.5 \text{ Hd}$ , are compared to the An-Hd isentrope determined in this study. It can be seen in Figure 8 that neither model is able to recover the An-Hd

isentrope, but that the Fa model does significantly worse. The Fa model also becomes unphysical at high pressure and lower temperature (Figure 8a), and this breaks the anticorrelation between errors in  $T$  and  $\rho$ , which are both underestimated, by 15% and 10% at 120 GPa, respectively (Figure 8b). The Hd model does significantly better with maximum errors at 120 GPa that overestimate  $T$  by 6% and underestimate  $\rho$  by 7% (Figure 8d). These errors worsen systematically for isentropes with progressively higher potential

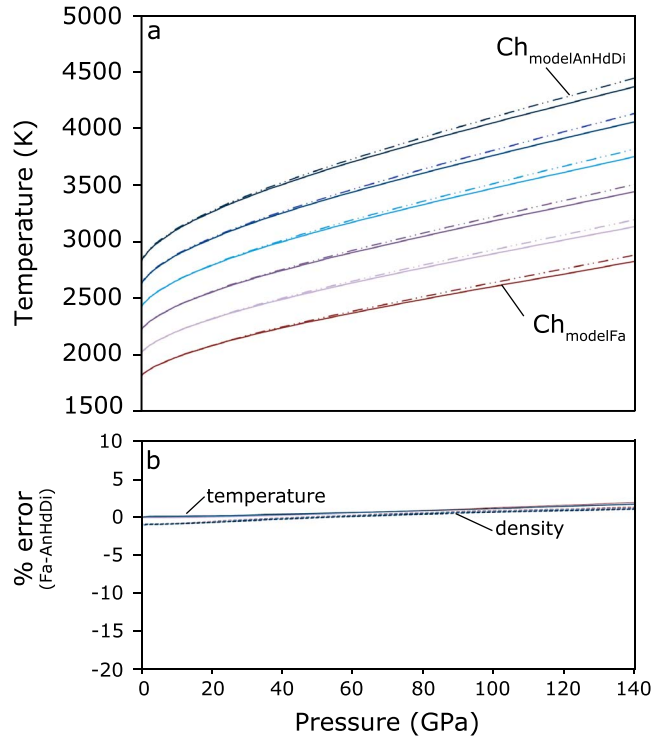


**Figure 11.** a) A comparison of the two mixing models for chondrite liquid ( $Ch_{\text{modelFa}} = 0.62 \text{ En} + 0.24 \text{ Fo} + 0.08 \text{ Fa} + 0.04 \text{ An} + 0.02 \text{ Di}$  and  $Ch_{\text{modelAnHdDi}} = 0.62 \text{ En} + 0.32 \text{ Fo} + 0.45 \text{ AnHdDi} - 0.12 \text{ An} - 0.28 \text{ Di}$ ) and b) their % error difference in temperature and density. Errors shown in text are the maximum at 120 GPa.

temperature (Figure 8c). These results are in line with our expectations based on 1 bar results: neither Fa nor Hd model can fully recover the behavior of the An-Hd isentrope, but closer similarity of  $V_{\text{FeO}}$  at 1 bar for Hd and An-Hd is significant enough to improve the fit at high pressure and temperature.

[33] Our third test examines the question: As FeO content decreases, does the difference between the end-member  $V_{\text{FeO}}$  and that of the model basalt still play as significant of a role in the final volume of the mixture at high pressure and temperature? We attempt to recover the isentrope of the model basalt, An-Hd-Di (which has less FeO than the previous An-Hd basalt), again using Fa and Hd end-member models:  $\text{AnHdDi}_{\text{modelFa}} = 0.33 \text{ An} + 0.667 \text{ Di} + 0.167 \text{ Fa} - 0.167 \text{ Fo}$  and  $\text{AnHdDi}_{\text{modelHd}} = 0.33 \text{ An} + 0.33 \text{ Hd} + 0.33 \text{ Di}$ . The results in Figure 9 show improvement for both models with the Fa model having high-pressure errors that underestimate  $T$  by 12% and underestimate  $\rho$  by 4% and the Hd model overestimating  $T$  by only 3% and underestimating  $\rho$  by 3%. Again, the Hd model does significantly better than the Fa model, likely due to the greater structural similarity of FeO in Hd and in An-Hd-Di at 1 bar. This test also suggests, at least in the studied region of CaO-FeO-MgO-Al<sub>2</sub>O<sub>3</sub>-SiO<sub>2</sub>, that the linear mixing approximation becomes better as the amount of FeO in the mixture decreases. That is, despite the variable behavior of  $V_{\text{FeO}}$ , there may be a threshold concentration of FeO below which this is negligible and the ideal solution approximation is adequate.

[34] We have chosen to perform these tests along isentropic paths since the corresponding temperature regimes are

more geologically relevant than the very high temperatures along a Hugoniot. Yet these same three tests can be performed along the Hugoniot of a liquid [c.f. *Asimow and Ahrens, 2010*] or any other chosen  $P$ - $T$  path.

[35] To show this, Figure 10 presents these tests performed along the calculated  $P$ - $T$  path for the intermediate liquid Hugoniot of Hd, An-Hd, and An-Hd-Di (Figures 10a, 10b, and 10c, respectively). Each diamond point corresponds to the EOS fit of an experimental point, and the error bars represent the average experimental error for that data set. A successful linear mixing model would reproduce the density within this given experimental error. Since each end-member Hugoniot (Fa, Fo, An, Di, and Hd) lies on its own separate  $P$ - $T$  path, a Mie-Grüneisen approximation is used to adjust the temperature to that of the given intermediate Hugoniot. This variable thermal pressure correction adds greater complexity in quantifying the error due to the temperature estimation, yet emphasizes that linear mixing of volumes is dependent on the chosen  $P$ - $T$  path as was shown previously for Fe-free liquids [*Asimow and Ahrens, 2010*]. This dependence can be seen in Figure 10a, which displays the density of Hd underestimated at all pressures along the Hugoniot whereas it was previously overestimated along the isentropic path (Figure 7). What is still captured though is the inability of the  $\text{Hd}_{\text{ModelFa}}$  to match the slope of the Hd Hugoniot as it was also unable to match the slope of the Hd isentrope (Figure 7). Likewise, mixing tests for An-Hd and An-Hd-Di Hugoniot (Figures 10b and 10c) give qualitatively similar results to their isentropic equivalent tests (Figures 8 and 9) in that there is an improvement in the linear mixing model as FeO content is decreased. In fact, the An-Hd-Di Hugoniot

can be approximated within the average experimental error (1.9%) using the linear combination of An, Hd, and Di volumes. Thus, as is true for the isentrope, it appears that an Fe-bearing end-member close in composition to the intermediate liquid of interest is needed for adequately predicting temperature and density along the Hugoniot.

[36] It still remains to define the best choice for  $V_{\text{FeO}}$  (i.e.,  $\text{Fe}^{2+}$  coordination state) for modeling a particular liquid composition in the mantle and to define the threshold FeO concentration below which this choice is unimportant. Our final test attempts to answer these questions by comparing the original chondrite model isentrope given in *Thomas et al.* [2012] that uses Fa as the  $V_{\text{FeO}}$  component ( $\text{Ch}_{\text{modelFa}} = 0.62 \text{ En} + 0.24 \text{ Fo} + 0.08 \text{ Fa} + 0.04 \text{ An} + 0.02 \text{ Di}$ ), and a model which uses An-Hd-Di as the  $V_{\text{FeO}}$  component ( $\text{Ch}_{\text{modelAnHdDi}} = 0.62 \text{ En} + 0.32 \text{ Fo} + 0.45 \text{ AnHdDi} - 0.12 \text{ An} - 0.28 \text{ Di}$ ). We again focus on isentropic  $P$ - $T$  paths as they are most geologically relevant. The results in Figure 11 show that the An-Hd-Di model predicts a slightly higher temperature but that models are within  $\pm 1.5\%$  for both  $T$  and  $\rho$ . Hence, the models are effectively indistinguishable, indicating that liquids with  $X_{\text{FeO}} \leq 0.06$  (chondrite model [Andraut et al., 2011]) can be suitably approximated with linear mixing. Mole fractions greater than this amount, such as An-Hd-Di ( $X_{\text{FeO}} = 0.08$ ), can be approximated within reasonable error ( $\pm 3\%$ ), but only when using an FeO component that has a similar  $V_{\text{FeO}}$  at 1 bar.

[37] Direct knowledge of the coordination state of  $\text{Fe}^{2+}$  in a given liquid thus is an important constraint on the volume behavior of that liquid, especially for high FeO contents. Conversely, precise data on the equation of state of an Fe-bearing liquid can be interpreted primarily as a constraint on the coordination state of  $\text{Fe}^{2+}$  in that liquid. However, liquids containing  $\text{Fe}_2\text{O}_3$ ,  $\text{Na}_2\text{O}$ ,  $\text{K}_2\text{O}$ , varying amounts of  $\text{SiO}_2$ , and other oxide species are far more complex than the five-component system studied so far. Other cations may influence the  $\text{Fe}^{2+}$  coordination state and may have variable coordination states themselves. In situ experiments analyzing cation coordination of complex glasses and melts at high pressure and temperature would greatly aid in elucidating these consequences and complementing macroscopic constraints from shock wave or other equation of state measurements.

## 5. Conclusions

[38] We completed 17 new preheated shock wave experiments on Hd, An-Hd, and An-Hd-Di liquids to determine the EOS of each composition. Having data on more compositions than are necessary to span the multicomponent oxide system, we applied these data to testing the validity of ideal mixing of volumes as a method of interpolation among end-member liquids. Ambient pressure density measurements on these and other Fe-bearing silicate liquids indicate that FeO has a molar volume (and therefore coordination state) that is highly dependent on composition [Guo et al., 2013], and our results show that this behavior extends to high pressure. An Fe-bearing end-member close in composition to the liquid of interest is necessary for adequately predicting temperature and density along its isentrope or Hugoniot. We find that deviations from linear mixing of volumes are significant at the level of several percent for liquid

mixtures with molar  $X_{\text{FeO}} > 0.06$  and are also dependent on the chosen  $P$ - $T$  path; therefore, caution should be taken when attempting to calculate densities of Fe-bearing liquids, being attentive to Fe content and  $P$ - $T$  conditions. On the other hand, densities and isentropic gradients for liquids in the system  $\text{CaO-FeO-MgO-Al}_2\text{O}_3\text{-SiO}_2$  with less than this threshold concentration of FeO can be approximated both at ambient and at high pressure using ideal volume of mixing.

[39] **Acknowledgments.** The authors would like to thank the following: the shock wave lab technical staff—Oleg Fat'yanov, Eprapodito Gelle, Russel Oliver, and Emma Dodd. Thanks to X. Guo and R. A. Lange for their ongoing collaboration and willingness to share their manuscripts. This work was supported by the National Science Foundation through award EAR-1119522.

## References

- Ahrens, T. J. (1987), *Shock Wave Techniques for Geophysics and Planetary Physics*, in *Methods in Experimental Physics*, edited by G. S. Charles, and L. H. Thomas, pp. 185–235, Academic Press, New York.
- Andraut, D., N. Bolfan-Casanova, G. L. Nigro, M. A. Bouhifd, G. Garbarino, and M. Mezouar (2011), Solidus and liquidus profiles of chondritic mantle: Implication for melting of the Earth across its history, *Earth Planet. Sci. Lett.*, *304*(1–2), 251–259.
- Asimow, P. D., and T. J. Ahrens (2010), Shock compression of liquid silicates to 125 GPa: The anorthite-diopside join, *J. Geophys. Res.*, *115*, B10209, doi:10.1029/2009JB007145.
- Asimow, P. D., D. Sun, and T. J. Ahrens (2008), Shock compression of preheated molybdenum to 300 GPa, *Phys. Earth Planet. In.*, *174*(1–4), 302.
- Bottinga, Y., and D. F. Weill (1970), Densities of liquid silicate systems calculated from partial molar volumes of oxide components, *Am. J. Sci.*, *269*(2), 169–182.
- Bottinga, Y., and D. F. Weill (1972), The viscosity of magmatic silicate liquids; a model calculation, *Am. J. Sci.*, *272*(5), 438–475.
- Bottinga, Y., D. Weill, and P. Richet (1982), Density calculations for silicate liquids. I. Revised method for aluminosilicate compositions, *Geochim. Cosmochim. Acta*, *46*(6), 909–919.
- Bottinga, Y., P. Richet, and D. F. Weill (1983), Calculation of the Density and Thermal-Expansion Coefficient of Silicate Liquids, *B. Minér.*, *106*(1–2), 129–138.
- Burns, R. G. (1993), *Mineralogical Applications of Crystal Field Theory*, 2nd ed., Cambridge University Press, Cambridge, UK, Cambridge Books Online. Web. 21 June 2013, doi:10.1017/CBO9780511524899.
- Canup, R. M. (2004), Simulations of a late lunar-forming impact, *Icarus*, *168*(2), 433–456.
- Canup, R. M. (2012), Forming a Moon with an Earth-like Composition via a Giant Impact, *Science*, *338*(6110), 1052–1055.
- Canup, R. M., and E. Asphaug (2001), Origin of the Moon in a giant impact near the end of the Earth's formation, *Nature*, *412*(6848), 708–712.
- Chase, M. W. (1998), NIST-JANAF Thermochemical Tables, 4th ed., *J. Phys. Chem. Ref. Data, Monogr.*, *9*, 1951 pp.
- Chen, G. Q., and T. J. Ahrens (Eds.) (1998), *Radio frequency heating coils for shock wave experiments*, 63–71 pp., Materials Research Society Symposia Proceedings, Warrendale, PA.
- Chen, G. Q., T. J. Ahrens, and E. M. Stolper (2002), Shock-wave equation of state of molten and solid fayalite, *Phys. Earth Planet. In.*, *134*(1–2), 35–52.
- Cooney, T. F., and S. K. Sharma (1990), Structure of glasses in the systems  $\text{Mg}_2\text{SiO}_4\text{-Fe}_2\text{SiO}_4$ ,  $\text{Mn}_2\text{SiO}_4\text{-Fe}_2\text{SiO}_4$ ,  $\text{Mg}_2\text{SiO}_4\text{-CaMgSiO}_4$ , and  $\text{Mn}_2\text{SiO}_4\text{-CaMnSiO}_4$ , *J. Non-Cryst. Solids*, *122*(1), 10–32.
- Ćuk, M., and S. T. Stewart (2012), Making the Moon from a Fast-Spinning Earth: A Giant Impact Followed by Resonant Despinning, *Science*, *338*(6110), 1047–1052.
- Garnero, E. J., and D. V. Helmberger (1995), A very slow basal layer underlying large-scale low-velocity anomalies in the lower mantle beneath the Pacific: Evidence from core phases, *Phys. Earth Planet. In.*, *91*(1–3), 161–176.
- Guo, X. (2013), Density and Compressibility of FeO-bearing Silicate Melt: Relevance to Magma Behavior in the Earth. Dissertation (Ph.D.), 194 pp., University of Michigan.
- Guo, X., R. A. Lange, and Y. H. Ai (2013), The density and compressibility of  $\text{CaO-FeO-SiO}_2$  liquids: Evidence for four-coordinated  $\text{Fe}^{2+}$  in the  $\text{CaFeO}_2$  component, *Geochim. Cosmochim. Acta*, doi:10.1016/j.gca.2013.06.007.

- Jackson, I., and T. J. Ahrens (1979), Shock wave compression of single-crystal forsterite, *J. Geophys. Res.*, *84*(B6), 3039–3048.
- Jackson, W. E., J. M. de Leon, G. E. Brown, G. A. Waychunas, S. D. Conradson, and J.-M. Combes (1993), High-Temperature XAS Study of Fe<sub>2</sub>SiO<sub>4</sub> Liquid: Reduced Coordination of Ferrous Iron, *Science*, *262*(5131), 229–233.
- Jackson, W. E., F. Farges, M. Yeager, P. A. Mabrouk, S. Rossano, G. A. Waychunas, E. I. Solomon, and G. E. Brown Jr. (2005), Multi-spectroscopic study of Fe(II) in silicate glasses: Implications for the coordination environment of Fe(II) in silicate melts, *Geochim. Cosmochim. Acta*, *69*(17), 4315–4332.
- Jeanloz, R. (1989), Shock Wave Equation of State and Finite Strain Theory, *J. Geophys. Res.*, *94*(B5), 5873–5886.
- Karki, B. B., D. Bhattarai, and L. Stixrude (2007), First-principles simulations of liquid silica: Structural and dynamical behavior at high pressure, *Phys. Rev. B*, *76*(10), 104,205.
- de Koker, N., B. B. Karki, and L. Stixrude (2013), Thermodynamics of the MgO–SiO<sub>2</sub> liquid system in Earth's lowermost mantle from first principles, *Earth Planet. Sci. Lett.*, *361*, 58–63.
- Lange, R. A. (1997), A revised model for the density and thermal expansivity of K<sub>2</sub>O–Na<sub>2</sub>O–CaO–MgO–Al<sub>2</sub>O<sub>3</sub>–SiO<sub>2</sub> liquids from 700 to 1900 K: extension to crustal magmatic temperatures, *Contrib. Mineral. Petrol.*, *130*(1), 1–11.
- Lange, R. A., and I. S. E. Carmichael (1990), Thermodynamic properties of silicate liquids with emphasis on density, thermal expansion and compressibility, *Rev. Mineral. Geochem.*, *24*(1), 25–64.
- Lange, R. A., and A. Navrotsky (1992), Heat capacities of Fe<sub>2</sub>O<sub>3</sub>-bearing silicate liquids, *Contrib. Mineral. Petrol.*, *110*(2–3), 311.
- Liu, Q., and R. A. Lange (2001), The partial molar volume and thermal expansivity of TiO<sub>2</sub> in alkali silicate melts: Systematic variation with Ti coordination, *Geochim. Cosmochim. Acta*, *65*, 2379–2393.
- Liu, Q., and R. A. Lange (2006), The partial molar volume of Fe<sub>2</sub>O<sub>3</sub> in alkali silicate melts: Evidence for an average Fe<sup>3+</sup> coordination number near five, *Am. Mineral.*, *91*, 385–393.
- Marsh, S. P. (Ed.) (1980), *LASL Shock Hugoniot Data*, 658 pp., University of California, Berkeley.
- Martin, G. B., M. S. Ghiorso, and F. J. Spera (2012), Transport properties and equation of state of 1-bar eutectic melt in the system CaAl<sub>2</sub>Si<sub>2</sub>O<sub>8</sub>–CaMgSi<sub>2</sub>O<sub>6</sub> by molecular dynamics simulation, *Am. Mineral.*, *97*(7), 1155–1164.
- Miller, G. H., T. J. Ahrens, and E. M. Stolper (1988), The equation of state of molybdenum at 1400 C, *J. Appl. Phys.*, *63*(9), 4469–4475.
- Miller, G. H., E. M. Stolper, and T. J. Ahrens (1991), The Equation of State of a Molten Komatiite 1 Shock Wave Compression to 36 GPa, *J. Geophys. Res.*, *96*(B7), 11,831–11,848.
- Mitchell, A. C., and W. J. Nellis (1981), Shock compression of aluminum, copper, and tantalum, *J. Appl. Phys.*, *52*(5), 3363–3374.
- Mo, X., I. S. E. Carmichael, M. L. Rivers, and J. F. Stebbins (1982), The partial molar volume of Fe<sub>2</sub>O<sub>3</sub> in multicomponent silicate liquids and the pressure-dependence of oxygen fugacity in magma, *Mineral. Mag.*, *45*(337), 237–245.
- Mysen, B. O. (1983), The structure of silicate melts, *Annu. Rev. Earth Planet. Sci.*, *11*(1), 75.
- Mysen, B. O. (1988), *Structure and Properties of Silicate Melts*, 368 pp., Elsevier Science, Amsterdam, doi:10.1016/0016-7037(89)90263-9.
- Nelson, S. A., and I. S. E. Carmichael (1979), Partial Molar Volumes of Oxide Components in Silicate Liquids, *Contrib. Mineral. Petrol.*, *71*(2), 117–124.
- Revenaugh, J., and S. A. Sipkin (1994), Seismic evidence for silicate melt atop the 410-km mantle discontinuity, *Nature*, *369*(6480), 474–476.
- Rigden, S. M., T. J. Ahrens, and E. M. Stolper (1984), Densities of liquid silicates at high pressures, *Science*, *226*(4678), 1071–1074.
- Rigden, S. M., T. J. Ahrens, and E. M. Stolper (1988), Shock compression of molten silicate: results for a model basaltic composition, *J. Geophys. Res.*, *93*(B1), 367–382.
- Rigden, S. M., T. J. Ahrens, and E. M. Stolper (1989), High-Pressure Equation of State of Molten Anorthite and Diopside, *J. Geophys. Res.*, *94*(B7), 9508–9522.
- Rossano, S., A. Y. Ramos, and J. M. Delaye (2000), Environment of ferrous iron in CaFeSi<sub>2</sub>O<sub>6</sub> glass; Contributions of EXAFS and molecular dynamics, *J. Non-Cryst. Solids*, *273*(1–3), 48–52.
- Ruoff, A. (1967), Linear Shock-Velocity-Particle-Velocity Relationship, *J. Appl. Phys.*, *38*(13), 4976.
- Shiraishi, Y., K. Ikeda, A. Tamura, and T. Saito (1978), On the viscosity and density of the molten FeO–SiO<sub>2</sub> system, *Trans. Jpn. Inst. Met.*, *19*, 264–274.
- Song, T.-R. A., D. V. Helmberger, and S. P. Grand (2004), Low-velocity zone atop the 410-km seismic discontinuity in the northwestern United States, *Nature*, *427*(6974), 530–533.
- Stebbins, J. F., I. S. E. Carmichael, and L. K. Moret (1984), Heat capacities and entropies of silicate liquids and glasses, *Contrib. Mineral. Petrol.*, *86*(2), 131–148.
- Thomas, C. W. (2013), Liquid silicate equation of state: Using shock waves to understand the properties of the deep earth. Dissertation (Ph.D.), 162 pp, California Institute of Technology.
- Thomas, C. W., Q. Liu, C. B. Agee, P. D. Asimow, and R. A. Lange (2012), Multi-technique equation of state for Fe<sub>2</sub>SiO<sub>4</sub> melt and the density of Fe-bearing silicate melts from 0 to 161 GPa, *J. Geophys. Res.*, *117*(B10), B10206, doi:10.1029/2012JB009403.
- Urbain, G., Y. Bottinga, and P. Richet (1982), Viscosity of liquid silica, silicates and aluminosilicates, *Geochim. Cosmochim. Acta*, *46*(6), 1061–1072.
- Williams, Q., and E. J. Garnero (1996), Seismic Evidence for Partial Melt at the Base of Earth's Mantle, *Science*, *273*(5281), 1528–1530.
- Zachariasen, W. H. (1932), The atomic arrangement of glass, *J. Am. Chem. Soc.*, *54*(10), 3841–3851.